IET Microwaves, Antennas & Propagation

Research Article

IET Journals
The Institution of Engineering and Technology

Dual-band frequency-reconfigurable MIMO PIFA for LTE applications in mobile hand-held devices

ISSN 1751-8725
Received on 14th October 2019
Revised 14th October 2019
Accepted on 14th January 2020
E-First on 17th February 2020
doi: 10.1049/iet-map.2019.0878
www.ietdl.org

Shruthi G.[1], *Choukiker Yogesh Kumar*[1] ✉

[1]*Department of Communication Engineering, School of Electronics Engineering, Vellore Institute of Technology, Vellore, TN, India*
✉ *E-mail: yogesh.ku.84@gmail.com*

Abstract: In this study, dual-port dual-frequency tuneable MIMO planar inverted-F antenna (PIFA) is presented for mobile hand-held device applications. The proposed MIMO antenna consists of two symmetrical PIFAs with the centre-to-centre distance of 43.0 mm ($0.1906\lambda_0$). The dual-band tunability is achieved by changing the capacitance (V_1 and V_2) of 4.15 pF (0 V)–0.72 pF (15 V). The impedance bandwidth of -6 dB is realised from 0.8 to 0.98 GHz for the lower band and 1.65 to 2.2 GHz for the higher band. The proposed antenna provides the independent frequency tunability without disturbing the frequency bands. It shows the good isolation for both the tuneable bands >20 dB without using any coupling element between the antenna structure. It has a peak realised gain of 3.44 dBi, good efficiency of $> 75\%$ and envelope correlation coefficient of 0.007. In addition, the proposed PIFA performance is analysed with total active reflection coefficient, channel capacity, diversity gain, multiplexing efficiency, mean effective gain and specific absorption ratio for the tuneable range of frequencies. The good agreement is obtained between simulation and experimental performances to validate the antenna parameters.

1 Introduction

There is a strong demand to support higher data rate transmission and better reliability in long-term evolution (LTE) wireless technology. The multiple-input multiple-output (MIMO) environment has the ability to fulfil the demand of increasing the wireless channel capacity and data rate without any additional power or spectrum [1]. However, one of the major challenges of employing MIMO systems in real work is the implementation of multiple antennas on a size-limited mobile terminal. The planar inverted-F antenna (PIFA) has been widely used as an internal antenna in the wireless communication system due to its wide band of operation, simple structure, good radiation patterns and easy integration with other active devices [2]. In addition, to cover more LTE bands, the impedance bandwidth of the MIMO antenna element with frequency reconfiguration has to be considered [3]. The reconfigurable PIFAs have been used in compact mobile handset devices, personal digital assistants, USB dongles and laptops to overcome the critical issue of decreasing the channel capacity, to compensate the mutual coupling takes place between the radiators [4].

In earlier work, indicated that two PIFAs are oriented above the ground plane using the air substrate, the inter antenna spacing should be greater to achieve more than 20 dB isolation [5]. Thus, designing a high-isolation MIMO antenna in a compact area remains a greater challenge. One of the most important requirements for a MIMO system is to reduce the mutual coupling between the adjacent antenna elements [6]. There are many practical methods to suppress the coupling in a MIMO antenna system includes a fractal-based EBG structures [7], defected ground plane structures gives bandgap filter characteristics which is one of the best way to reduce the coupling takes place between the antennas [8], neutralisation technique to enhance the port-to-port isolation [9], planar soft surfaces used to decrease the coupling level [10], a compact planar spiral line (PSL) is employed to achieve isolation enhancement [11], a T-shaped decoupling slot is inserted in the ground plane for high isolation [12]. As a result, efficient isolation enhancement techniques are highly required for integrated MIMO devices.

The MIMO reconfigurable PIFA incorporating cognitive radio (CR) techniques is effective for spectrum utilisation along with improving the channel capacity and data reliability. In [13], planar meandered reconfigurable F-shaped MIMO was investigated to cover the wide frequency bands below 1 GHz, which is suitable in CR-based wireless hand-held devices. Here, The rectangular defected ground structure (DGS) was used for isolation enhancement between the antenna elements. The multi-band reconfigurable MIMO antennas and UWB sensing antenna with low operating frequency without any additional planar structure for CR applications were investigated for the different RF spectrum [14]. It covers the wide frequency sweep over multibands using the varactor diodes, found to be suitable for tablet PC applications in the second generation CR platforms [15].

The PIFA exhibits the low SAR and reduces backward radiation towards the human head. The MDNC substrate is excellent for antenna miniaturisation [16] as well as reducing the SAR (0.7224 W/kg) to show the desired performance. The dual-element LTE MIMO antenna provides the guidelines to design the antenna showing the optimised SAR (2.7 W/kg) performance for LTE mobile phones [17]. In [18], the integration of PIFA and a capacitive grating AMC conductor was presented for an SAR reduction in the penta-band mobile terminals. This conductor can be able to block the radiation pattern towards the head without reducing the antenna efficiency. The reconfigurable PIFA with a parasitic strip line for the hepta-band WWAN and LTE has been discussed with SAR (1.402 W/kg) distribution. The fundamental resonance of the antenna can be easily controlled using reconfiguration technique [19]. The effects of the human hand and head on the SAR (1.262 W/kg) values and antenna performances have been investigated using mobile handset of PIFA [20]. The effect of SAR highly concentrates on hand model than the head model. A quad-element multi-wideband antenna array was demonstrated for LTE MIMO mobile terminals [21]. Using the adaptive concept, the MIMO channel performance can be enhanced for three kinds of user effects, namely, specific anthropomorphic mannequin (SAM) head (4.2 W/kg) and personal digital assistants (PDA) hand (talk mode), PDA hand (data mode), and dual hands (read mode) for the improvement of MIMO channel capacity with user effects. The gain and radiation efficiency of MIMO antenna is improved by loading CRLH antenna with SRR and CSRR [22]. When the inter-element spacing greater than critical distance, the better impedance matching is achieved which reduces the ECC and enhances the total efficiency of the antenna [23].

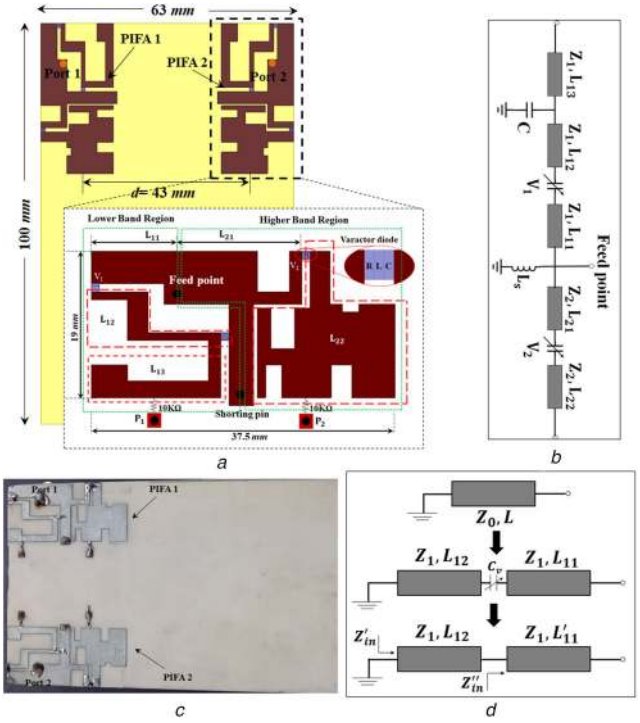

Fig. 1 *Geometry of the proposed MIMO reconfigurable antenna*
(a) MIMO PIFA main geometry with zoom view of radiating element, ***(b)*** PIFA transmission line model, ***(c)*** Tuneable part transmission line model, ***(d)*** Fabricated prototype of proposed PIFA

In this communication, we are reporting the printed MIMO reconfigurable PIFA employed on the edges of the substrate and loaded with a varactor diode to operate at dual LTE frequency bands. This MIMO antenna optimises the isolation characteristics with a full ground plane. Here, the antenna prototype is designed in such a way, the spacing between the elements is enough for isolation enhancement without using decoupling slots in the ground plane. The patch geometry is divided into two regions: lower band (LB) and higher band (HB). The varactor diodes are used between these regions to tune the PIFA operating bands. The LB region tunes from 0.8 to 0.98 GHz and HB region tunes from 1.65 to 2.2 GHz. It has good isolation (>20 dB), low envelope correlation coefficient (0.007), acceptable channel capacity loss of 0.3 bits/s/Hz and high diversity gain (>9 dB) for MIMO environment. Further, the SAR analysis of human head and hand model also studied. The detailed simulation and experimental results for the proposed MIMO antenna are presented and analysed.

2 Antenna geometry and performance

The configuration of the proposed printed MIMO dual-band frequency tuneable PIFA for mobile devices is shown in Fig. 1*a* with the zoom view of the radiating element. The PIFAs are symmetrically arranged and separated by 43 mm ($0.1906\lambda_0$) distance from centre-to-centre, which is less than the distance of $0.5\lambda_0$ required for mutual coupling reduction without decoupling slots added into the ground plane. The radiating elements are integrated at the top edge corners of the RO4003C substrate ($100 \times 63 \times 1.524$ mm^3) with a relative permittivity of $\varepsilon_r = 3.55$, a thickness of 1.524 mm and loss tangent ($\tan\delta$) of 0.0027 and fed by 50 Ω coaxial feed for impedance matching. The overall size of the ground plane is 100×63 mm^2 for mobile phone applications. The size of the radiating element is chosen to be 37.5×19 mm^2 and calculated with the transmission line model as shown in Figs. 1*b* and *c*. To investigate the performance of the proposed MIMO PIFA structure, the simulation is carried out using Ansys HFSS v18 and experimentally verified. The fabricated prototype of the proposed MIMO frequency reconfigurable PIFA is shown in Fig. 1*d*.

2.0.1 Antenna design

The radiating element of the proposed antenna is divided into two arms: main arm and supporting arm. The T-shaped radiator acts as the main arm and performs dual-band operation. It is shorted to the ground plane, makes the antenna compact to resonate at quarter wavelength as well as to reduce the coupling effect with other elements. The main objective of the proposed work is to design the PIFA for LTE frequency bands hence the supporting arms are used with the main arm. The supporting arms (L_{12}, L_{13} and L_{22}) cover the desired dual-band frequency, increase the electrical length of the antenna and makes the antenna reconfigurable. For the proposed PIFA geometry, the supporting arms L_{12} and L_{13} along with the main arm is considered as a LB region. Similarly, the other supporting arm L_{22} along with the main arm is considered as a HB region. To reduce the effect of coupling between the main arm and supporting arms, a fixed capacitor is integrated into the antenna. To make the antenna as a frequency tuneable PIFA, the varactor diodes are used [24]. A 10 kΩ resistor is used in the LB and HB regions to bias the varactor diodes at the point P_1 and P_2. The geometry of the radiating element is shown with the zoom view in Fig. 1*a*. When the varactor diodes (Skyworks SMV1232-079LF), ($C = 4.15$–0.72 pF, R_s=1.5 Ω, $L = 0.7$ nH) [25] are embedded in the LB and HB regions of PIFA, the electrical length of the antenna will be increased simultaneously for shifting the resonance to higher frequencies. As a result, the lower frequency band tuning and higher band tuning of (0.8–0.98 GHz) and (1.65–2.2 GHz) are achieved, respectively. These two symmetrically designed PIFAs employed as diversity antennas operating at the same frequency bands.

The radiating element of the proposed antenna is designed based on the transmission line model as shown in Fig. 1*b* and evaluated with the equations given in [26]. They are modelled with the characteristic impedance (Z_0) and input impedance (Z_{in}) is given below:

$$Z_0 = \frac{120\pi}{\sqrt{\varepsilon_{reff}}\left\{\frac{W_0}{h} + 1.393 + 0.667\ln\left[\frac{W_0}{h} + 1.444\right]\right\}}, \quad \frac{W_0}{h} > 1 \tag{1}$$

where h is the height of the substrate and W_0 is the width of the section for the proposed geometry. The impedance of the LB and HB sections is considered as $Z_1 = Z_2 = Z_0$.

$$Z_{in} = Z_0\left\{\frac{Z_L + jZ_0\tan\beta l}{Z_0 + jZ_L\tan\beta l}\right\} \tag{2}$$

and

$$\beta = \frac{2\pi}{\lambda} \tag{3}$$

where Z_L and β are the load impedance and propagation constant, respectively. The βl is the electrical length of the transmission line and it is considered as $\lambda/4$. The $C = 1.5$ pF and L_S=0.71 nH are used as a fixed capacitor to avoid the coupling between the sections and a fixed inductor to capture the inductive effect (X_S) of the shorting pin in the transmission line model, respectively. The inductive effect (X_S) is written as follows:

$$X_S = X_P = \frac{\eta_0\omega h}{2\pi C}\left\{\frac{4c}{\xi\omega d\sqrt{\varepsilon_r}}\right\} \tag{4}$$

where ξ is the Euler's constant, d is the diameter of feeding probe and shorting pin, c is the speed of light and η_0 is the free space intrinsic impedance. We can assume that the inductive effect of the feed pin (X_P) is same as the inductive effect of the shorting pin (X_S).

Fig. 1*c* shows the equivalent circuit model for PIFA with series tuning capacitor C_v. It can be used to demonstrate the mechanism of tuneable frequency for the designed PIFA. Here, Z'_{in} and Z''_{in} are

Table 1 Extracted values of transmission line for the proposed MIMO reconfigurable PIFA

Parameters	Sections				
	L_{11}	L_{12}	L_{13}	L_{21}	L_{22}
impedance, Ω	$Z_1 = 47.2$	$Z_1 = 35.93$	$Z_1 = 32.15$	$Z_2 = 33.93$	$Z_2 = 15.12$
electrical length, deg.	15.9	30.6	29	28.5	32.1
length, mm	9	17	16	15.75	17
width, mm	4	6	7	6.5	18

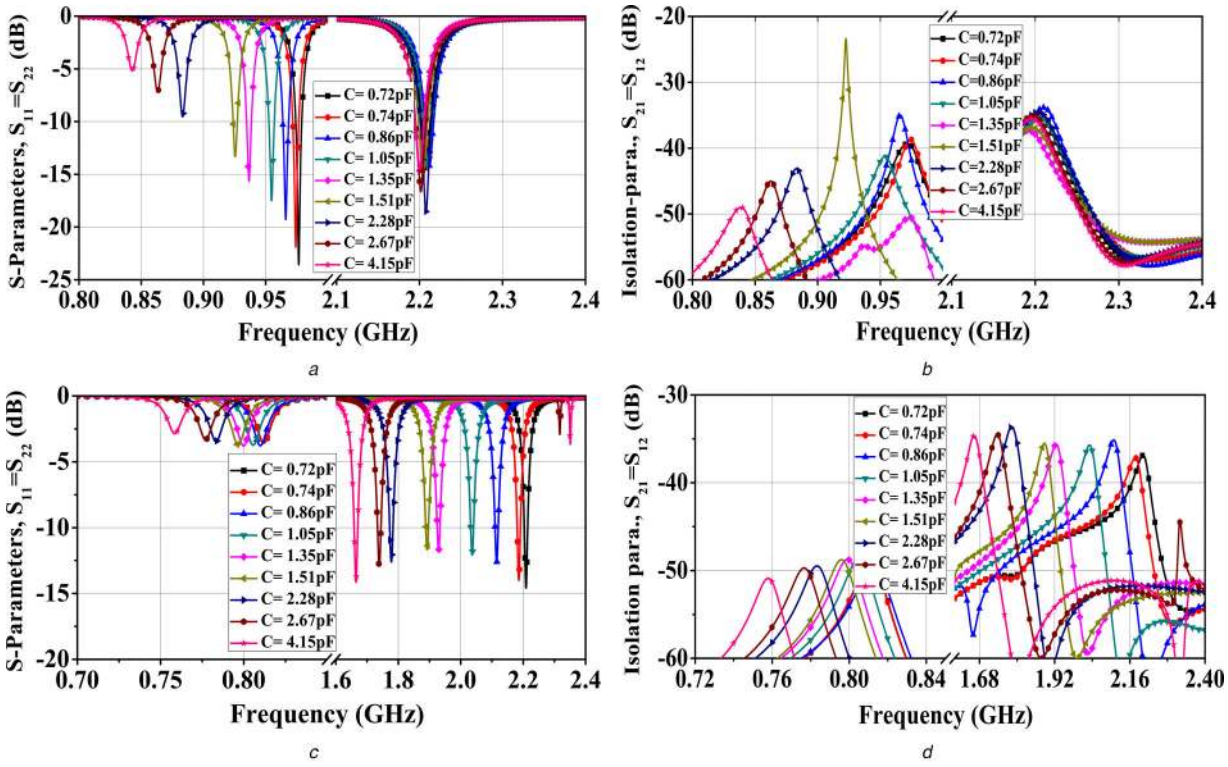

Fig. 2 *Simulated S-parameters and isolation parameters of the proposed MIMO reconfigurable PIFA for different capacitance of varactor diode*
(a) S-parameters ($S_{11} = S_{22}$) for LB tuning, ***(b)*** Isolation parameters ($S_{12} = S_{21}$) for LB tuning, ***(c)*** S-parameters ($S_{11} = S_{22}$) for HB tuning, ***(d)*** Isolation parameters ($S_{12} = S_{21}$) for HB tuning

the input impedances of the short-circuited transmission line model. For this PIFA, the Z'_{in} assumes to be zero for short-circuit open-end and Z''_{in} can be written as follows:

$$Z''_{in} = \frac{1}{j\omega C_v} + \frac{Z_1}{j\tan(\beta L_{11})} \tag{5}$$

and

$$Z''_{in} = \frac{1}{j} Z_1 \tan(\beta L'_{11}) \tag{6}$$

by equating (5) and (6)

$$L'_{11} = \frac{1}{\beta}\tan^{-1}\left\{\frac{Z_1\omega C_v \tan(\beta L_{11})}{\tan(\beta L_{11}) + Z_1\omega C_v}\right\} \tag{7}$$

where L'_{11} and L_{11} represent the new length and physical length of the transmission line, respectively. With the help of series tuning capacitor C_v, the centre frequency (f_c) can be calculated as follows:

$$f_c = \sqrt{f_{max} f_{min}} \tag{8}$$

Here f_{max} is the maximum resonant frequency and f_{min} is the minimum resonant frequency. It is obtained with variable capacitance values of C_{max} and C_{min} for different Z_0 values. The $Z_1 = Z_2$ assumption is used to simplify the analysis. Finally, with the use of centre frequency, the impedances, the length, and width of each quarter wavelength sections realised in the microstrip configuration are extracted and listed in Table 1. Also, from (1) to (8), we will be able to evaluate the tuning range of the proposed PIFA.

2.0.2 Simulation results

Based on the extracted values from the transmission line model, the proposed reconfigurable PIFA is designed and placed in the MIMO configuration with centre-to-centre distance of 43 mm. Fig. 2 shows the simulated S-parameters ($S_{11} = S_{22}$) and isolation parameters ($S_{12} = S_{21}$) of the proposed MIMO reconfigurable antenna for LB and HB frequency tunabilities. The variable capacitance value of the varactor diode decreases, the resonant frequency shifted towards higher frequency. Figs. 2*a* and *b* show the S-parameters and isolation parameters for LB frequency tuning. It is observed that by varying the capacitance of varactor diode (V_1) from 4.15 to 0.72 pF and V_2 kept constant at lower value of 0.86 pF. As a result, the centre frequency of LB tunes from 0.8 to 0.98 GHz (22%). Similarly, when the varactor diode (V_2) is tuned by varying the capacitance from 4.15 to 0.72 pF and V_1 kept constant at higher value of 4.15 pF. The centre frequency of higher band is tuned from 1.65 to 2.2 GHz (30%). It is noted that the S-parameters ($S_{11} = S_{22}$) and isolation parameters ($S_{12} = S_{21}$) results for both ports 1 and 2 in MIMO configuration are similar in nature. Hence, S_{11} and S_{22} are overlapped, similarly the S_{12} and S_{21} are also overlapped. The −6 dB impedance bandwidth is realised for both LB and HB tunings. Also, the isolation parameters are well below 20 dB as expected for mutual coupling between both the ports. It is concluded that both

the bands are shifted towards higher frequency with decreasing the capacitance of a varactor diode.

Figs. 3*a* and *b* show the analysis of surface current distribution between port 1 and port 2 for isolation in the MIMO PIFA configuration at LB and HB frequencies. When port 1 is excited and port 2 is terminated in 50 Ω and vice versa, it is noticed that there is no current in the other port of PIFA. Hence, it indicates that the isolation between both the ports is well suited for the MIMO configuration. In addition, these figures also indicate the current distribution at LB (0.9 GHz) and HB (1.7 GHz), for the reconfigurable MIMO PIFA. It is observed that at lower frequency (0.9 GHz), the current is distributed in the LB tuning section. At the same time, no current is realised in the HB section. Similarly, at higher frequency (1.7 GHz), the current is distributed in the HB section and some amount of current is penetrated in LB tuning section, as shown in Fig. 3*a*. This is due to the higher resonance of the LB PIFA section coincides with the lower resonance of the HB PIFA section. The same results are obtained when port 2 is excited at 0.9 and 1.7 GHz because of the symmetrical structure of PIFA as shown in Fig. 3*b*.

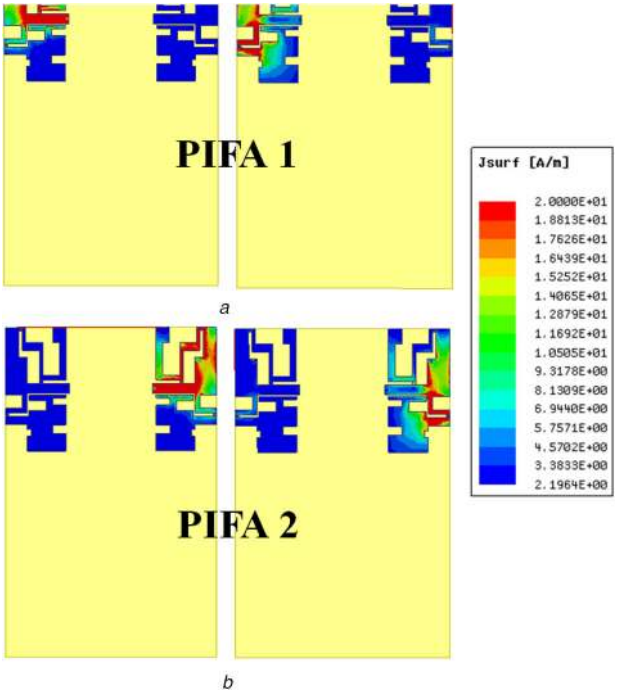

Fig. 3 *Surface current distribution of the proposed MIMO reconfigurable PIFA*

(a) Port 1 is excited for 0.9 and 1.7 GHz, ***(b)*** Port 2 is excited for 0.9 and 1.7 GHz

Figs. 4*a* and *b* shows the simulated 3D radiation pattern of the proposed MIMO reconfigurable PIFA antenna at lower tuneable frequencies of (0.8 and 0.98 GHz) and higher tuneable frequencies of (1.65 and 2.2 GHz). It can be seen that the gain of the proposed PIFA at all the frequencies within the bands are more than 2.5 dBi. The 3D patterns are omnidirectional towards the lower tuneable frequency band and becomes nearly omnidirectional with multiple lobes towards the higher tuneable frequency band.

3 Experimental verification

The proposed MIMO reconfigurable PIFA is milled on the copper side of RO4003C substrate using LPKF-42 Protomat milling machine. The photographs of fabricated antenna are shown in Fig. 1*d*. The antenna is measured using Anritsu vector network analyser (VNA) for an impedance matching. The radiation patterns were measured in an anechoic chamber, both available at the antenna and microwave laboratory (AML) at VIT University. The measured values of the S-parameters ($S_{11} = S_{22}$) and isolation parameters ($S_{12} = S_{21}$) are plotted in Figs. 5*a–d* for port 1 and port 2 in the MIMO reconfigurable PIFA configuration at LB and HB frequencies. It is observed that increasing the bias voltage of varactor diode from 0 to 15 V, the resonance frequencies shifted towards the higher frequency for both the bands. For tuning the LB, the bias voltage of varactor diode (V_1) varies from 0 to 15 V and V_2 kept at any constant value between 0 and 15 V, and vice versa. As a result, the resonant frequency of the LB section tuned from 0.8 to 0.98 GHz (22%) and HB section tuned from 1.65 to 2.2 GHz (30%) for the impedance bandwidth of −6 dB. These results exhibit reasonable agreement, although there is a frequency shift that can be attributed to reflection from SMA connector and some uncertainty in the electrical properties of the substrate. The bandwidths achieved meet the requirements of 0.8–0.980 and 1.65–2.2 GHz for mobile hand-held device applications. The isolation between the two antennas is better than 30 and 35 dB for the lower and higher frequency bands, respectively.

Figs. 6*a* and *b* show the measured normalised radiation patterns of the proposed PIFA for LB and HB frequencies, respectively. The E_θ and E_ϕ patterns are taken to predict the behaviour in *XZ* (Co-pol. and X-pol.)-plane and *YZ* (Co-pol. and X-pol.)-plane. During the measurement, only port 1 of PIFA is excited while port 2 of PIFA is terminated with a 50 Ω load. It is observed that the patterns are omnidirectional in tuning band for both LB and HB tuning frequencies. It can be concluded that the performance of the PIFA

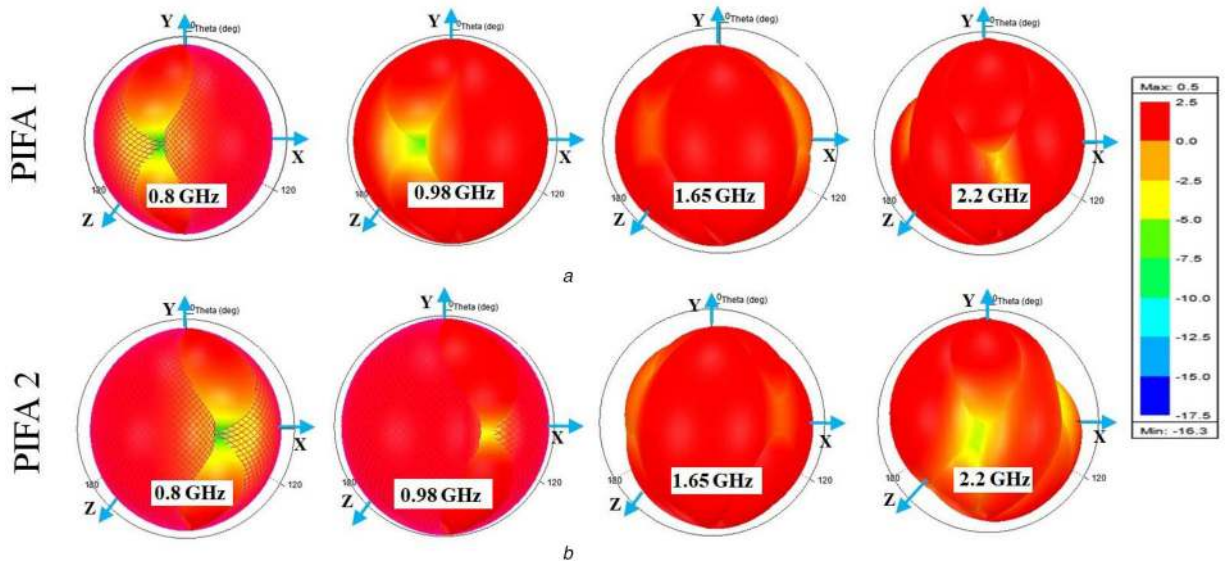

Fig. 4 *3D radiation pattern of the proposed MIMO reconfigurable PIFA*

(a) Port 1@ PIFA 1 at: lower tuneable band 0.8 and 0.98 GHz, higher tuneable band 1.65 and 2.2 GHz, ***(b)*** Port 2@ PIFA 2 at: lower tuneable band 0.8 and 0.98 GHz, higher tuneable band 1.65 and 2.2 GHz

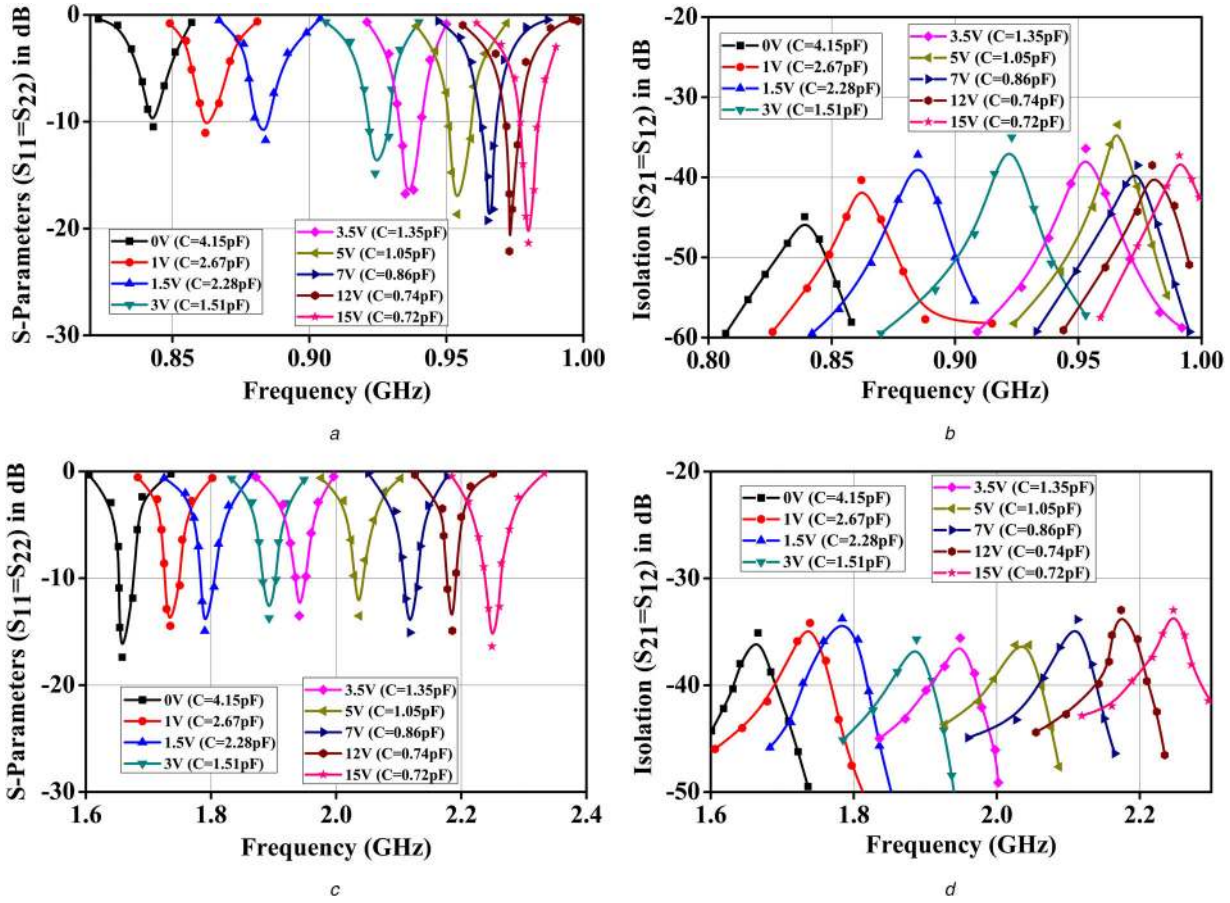

Fig. 5 *Measured S-parameters and isolation parameters of the proposed MIMO reconfigurable PIFA for different capacitance of varator diode*
(a) S-parameters ($S_{11} = S_{22}$) for LB tuning, ***(b)*** Isolation parameters ($S_{12} = S_{21}$) for LB tuning, ***(c)*** *c* S-parameters ($S_{11} = S_{22}$) for HB tuning, ***(d)*** Isolation parameters ($S_{12} = S_{21}$) for HB tuning

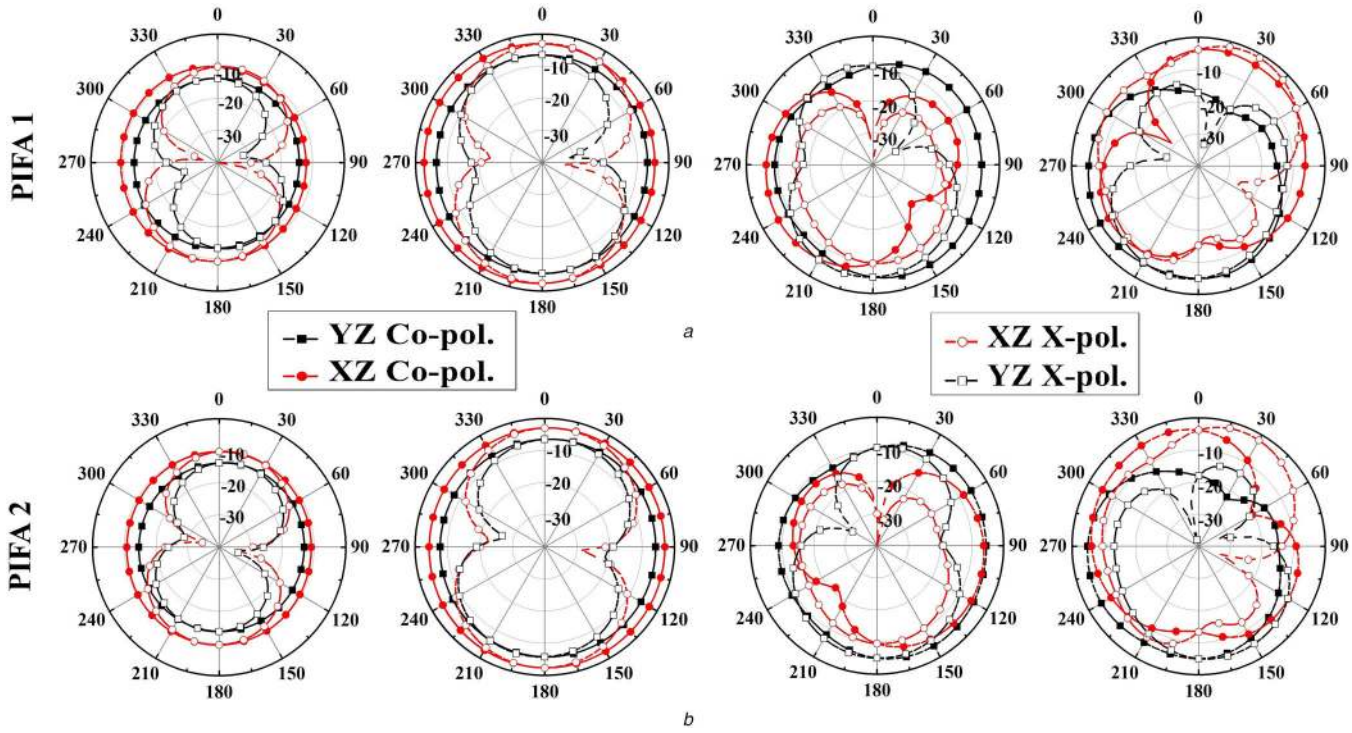

Fig. 6 *Measured radiation pattern of the proposed MIMO reconfigurable PIFA*
(a) Port 1 @ PIFA 1 at: lower tuneable band 0.8 and 0.98 GHz, higher tuneable band 1.65 and 2.2 GHz, ***(b)*** Port 2 @ PIFA 2 at: lower tuneable band 0.8 and 0.98 GHz, higher tuneable band 1.65 and 2.2 GHz

for both reverse and forward bias conditions is well matched for uniform power levels. In the proposed MIMO reconfigurable PIFA configuration, the radiators are placed symmetrically, therefore, it will provide complementary or diversity patterns when one antenna port is excited at a time and the other one is matched terminated.

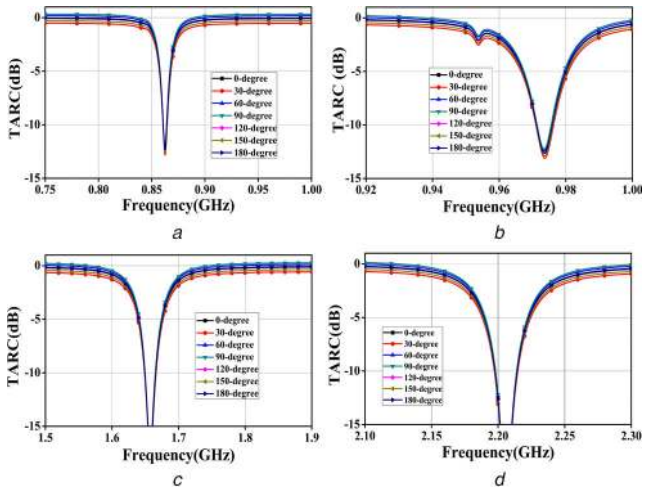

Fig. 7 *Computed TARC of the proposed MIMO reconfigurable PIFA*
(a) 0.86 GHz (LB tuning), ***(b)*** 0.97 GHz (LB tuning), ***(c)*** 1.65 GHz (HB tuning), ***(d)*** 2.2 GHz (HB tuning)

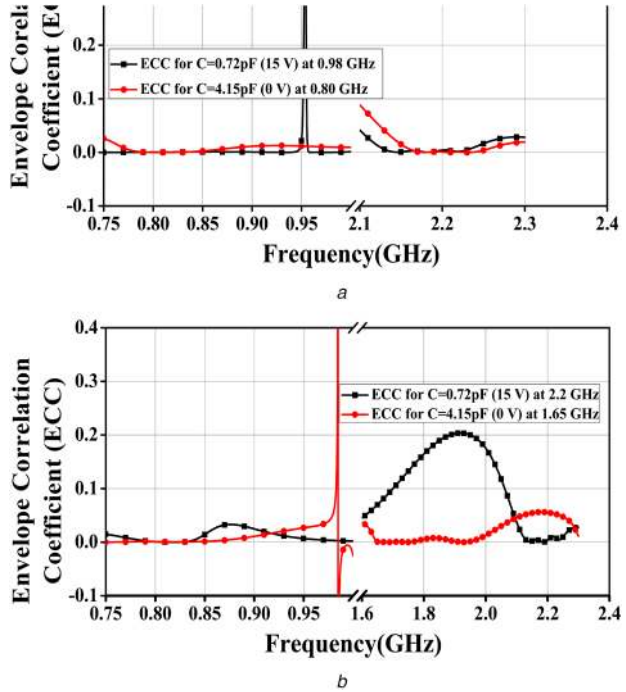

Fig. 8 *ECC of the proposed MIMO reconfigurable antenna*
(a) LB tuning frequency, ***(b)*** HB tuning frequency

4 Diversity performance of MIMO reconfigurable PIFA

The diversity performance of the proposed MIMO reconfigurable antenna is computed with the parameters such as total active reflection coefficient (TARC), envelope correlation coefficient (ECC), mean effective gain (MEG), diversity gain (DG), channel capacity loss (CCL) and multiplexing efficiency.

The TARC relates the total incident power to the total outgoing power in an N-port microwave component. The TARC is mainly used for MIMO antenna systems and array antennas, where the outgoing power is unwanted reflected power. TARC can be evaluated for the proposed reconfigurable MIMO system by the relation [27]

$$\text{TARC} = \frac{\sqrt{(|S_{11} + S_{12}e^{j\theta}|^2) + (|S_{21} + S_{22}e^{j\theta}|^2)}}{\sqrt{2}} \tag{9}$$

where θ is the feed phase difference of each excited signals of MIMO antenna. The phase difference varies from 0° to 180° with equal intervals of 30°. The TARC performance of the proposed MIMO antenna is calculated at two tuneable frequencies for both the LB (0.86 and 0.97 GHz) and HB (1.65 and 2.2 GHz) are shown in Figs. 7*a–d*. The shape of TARC graph has a slight deviation from the original antenna return loss due to the effect of increased mutual coupling. The TARC values are found to be in good agreement with reflection coefficient (S-parameters) parameter of the antenna S_{11}/S_{22}.

Next, in the MIMO environment ECC and MEG will give the deterministic and the channels statistical parameters for multi-antenna system. The ECC can be evaluated from the correlation between the radiation patterns of multiple antenna elements. For analysis of ECC, all incoming multipath fields arrive from a uniform propagation environment is assumed to be $\theta = \pi/2$ and the cross-polarisation discrimination (XPD) is assumed to be unity ($\Gamma = 1$). The ECC can be characterised by the following equation [13]:

$$\rho_{e_{ij}} = \frac{\int_0^{2\pi}\int_0^{\pi} A_{ij}(\theta,\phi)\sin\theta\,\mathrm{d}\theta\,\mathrm{d}\phi}{\sqrt{\int_0^{2\pi}\int_0^{\pi} A_{ii}(\theta,\phi)\sin\theta\,\mathrm{d}\theta\,\mathrm{d}\phi}\cdot\sqrt{\int_0^{2\pi}\int_0^{\pi} A_{jj}(\theta,\phi)\sin\theta\,\mathrm{d}\theta\,\mathrm{d}\phi}} \tag{10}$$

where

$$A_{ij} = \Gamma\cdot E_{\theta i}(\theta,\phi)E^*_{\theta j}(\theta,\phi)P_\theta(\theta,\phi) + E_{\phi i}(\theta,\phi)E^*_{\phi j}(\theta,\phi)P_\phi(\theta,\phi) \tag{11}$$

where $E_{\theta,\phi}(\theta,\phi)$ is the complex electric far-field component association with the antenna element 'i'. $P_{\theta,\phi}(\theta,\phi)$ is the power angular density function of the incoming plane waves in the θ and ϕ polarisation. The Γ is the XPD of the incident multipath field and it is written in terms of vertical to horizontal time-average power ratio as follows:

$$\text{XPD} = \frac{P_\text{v}}{P_\text{h}} \tag{12}$$

For the proposed MIMO reconfigurable PIFA, the ECC can be evaluated as < 0.007 and < 0.003 for LB and HB tuneable frequencies which is well matching with the measured values of < 0.054 and < 0.044. The measured ECC is shown in Figs. 8*a* and *b*.

4.1 Mean effective gain

In MIMO environment, the MEG is defined as the ratio of mean received power (P_rec) of an antenna to the mean incident power (P_inc) of the same antenna along the vertically and horizontally polarised waves received by an isotropic antenna [5] and expressed as follows:

$$\text{MEG}_i = \frac{P_\text{rec}}{P_\text{inc}} \tag{13}$$

(see (14))

where $G_{\theta\phi}(\theta,\phi)$ is the gain pattern for the 'ith' element. For the uniform propagation environment XPD=1 and $P_\theta = P_\phi = 1/4\pi$, the MEG of an element is equal to half of its total radiation efficiency (e^i_tot) and can be represented as

$$= \int_0^{2\pi}\int_0^{\pi} \frac{\text{XPD}\cdot G_{\theta i}(\theta,\phi)\cdot P_\theta(\theta,\phi) + G_{\phi i}(\theta,\phi)\cdot P_\phi(\theta,\phi)}{1+\text{XPD}}\sin\theta\,\mathrm{d}\theta\,\mathrm{d}\phi \tag{14}$$

$$\mathrm{MEG}_i = \frac{e^i_{\mathrm{tot}}}{2} \tag{15}$$

and

$$e^i_{\mathrm{tot}} = \int_0^{2\pi}\int_0^{\pi} G_{\theta i}(\theta,\phi) + G_{\phi i}(\theta,\phi)\sin\theta\,\mathrm{d}\theta\,\mathrm{d}\phi \tag{16}$$

For a good diversity performance, the MEG ratio ($|\mathrm{MEG}_i|/|\mathrm{MEG}_j|$) and MEG difference ($|\mathrm{MEG}_i| - |\mathrm{MEG}_j|$) of the multiple antennas in the MIMO system should approach unity and zero, respectively and should lie within ±3 dB. It indicates that the branch signals are as independent as possible from each other, and the power is delivered almost equally to all the branches. As expected for the proposed MIMO reconfigurable PIFA, the MEG values (MEG_1 and MEG_2) are similar at each frequency of interest at both LB and HB tuning as shown in Table 2. The slight difference between MEG_1 and MEG_2, considering the fact that the two antennas are identical, is due to the difference in the gain patterns at the assumed angle for the incident power. In addition, this MEG_1 and MEG_2 ratio also defines the power imbalance of two ports. This power imbalance leads to degradation of diversity gain for the MIMO environment and written as

$$\mathrm{DG} = 10\sqrt{1-\rho_e^2}\cdot k \tag{17}$$

The DG can be calculated in dB and k is the MEG ratio. Thus MEG gain should be required as 1 for good DG [28]. It is noted that the proposed antenna has diversity gain (DG > 9 dB) for the entire operating frequency range. The calculated values of DGs are found to be 9.98 and 10 dB for the LB tuning and HB tuning, respectively. This dual-feed reconfigurable PIFA can therefore be used as a diversity/MIMO antenna in wireless applications.

Similarly, capacity loss (bits/s/Hz) is another performance parameter which characterises the quality of a MIMO antenna system. Channel capacity is the tightest upper bound on the rate of information that can be reliably transmitted over a communications channel. This can be defined using the correlation matrix given in [29], and is calculated by using (18), which is found to be below 0.4 bits/s/Hz

$$C_{\mathrm{loss}} = -\log_2 \det(\Psi^R) \tag{18}$$

where Ψ^R is the receiving antenna correlation matrix and expressed as follows:

$$\begin{aligned} \Psi^R &= \begin{bmatrix} \rho_{ii} & \rho_{ij} \\ \rho_{ji} & \rho_{jj} \end{bmatrix}, \\ \rho_{ii} &= 1 - (|S_{ii}|^2 + |S_{ij}|^2), \\ \rho_{ij} &= -(S^*_{ii}S_{ij} + S^*_{ji}S_{ij}) \\ &\quad \text{for } i = 1, 2, 3, \ldots \end{aligned} \tag{19}$$

In Table 2, the comparison of measured and simulated capacity loss values of the proposed MIMO antenna. It is observed that the capacity loss does not exceed 0.3 bits/s/Hz and it is well below the threshold value 0.4 bits/s/Hz for both the LB tuning and HB tuning for the proposed MIMO reconfigurable PIFA. In the spatial mode of operation to achieve the optimum antenna system design, multiplexing efficiency [21] is evaluated for the proposed MIMO reconfigurable PIFA. It is noted that for the proposed antenna design, the simulated multiplexing efficiencies of the LB ranges from −3 to −7 dB and the HB ranges from −1.5 to −5 dB. All the measured and simulation of diversity performance for the proposed MIMO reconfigurable antenna are summarised in Table 2. Table 3 shows the performance of the proposed MIMO PIFA with previously selected references. It is concluded that the proposed antenna can be used for modern mobile hand-held devices.

5 SAR performance of the MIMO reconfigurable PIFA

The SAR is an important criterion to examine the health risks of electromagnetic absorption in the human body for mobile devices. It is computed as

$$\mathrm{SAR} = \frac{\sigma}{2\rho}\left|E\right|^2 \tag{20}$$

where ρ (kg/m^3) and σ are the body tissue density and conductivity, respectively. E (V/m) is the root-mean-square (rms) value of the electric field strength in the tissue. The SAM phantom model for head and hand as shown in Figs. 9*a* and *b* for the proposed MIMO reconfigurable PIFA. The PIFA is placed at an angle of ≅ 45°, at a distance of 15 mm over 1 g of the human tissue mass, which is the voice position for the mobile device based on the IEEE Std. 1528 [30]. To investigate the effect of hand model, one hand scenario with an antenna orientation of 0° is chosen. Figs. 10*a–d* show the human head and hand model SAR performances for both LB (0.86 and 0.98 GHz) and HB (1.72 and 2.20 GHz) tuneable frequencies. Here, 24 and 21 dBm taken as an input power of the proposed model to determine the SAR values [19]. It is observed that the SAR in the human head and hand models has a maximum value of 0.26627 and 0.5198 W/kg, respectively. It is noticed that the higher amount of SAR is fundamentally concentrated in the hand at a lower tuneable frequency and less amount in the higher tuneable frequency. Table 4 shows the SAR values and *E*-field distribution of different frequencies, the distance from the head and one-hand scenario hand models of the proposed MIMO reconfigurable PIFA. The SAR and *E*-field intensity are more for the LB compared to the HB tuneable frequencies. This may be due to the larger penetration depth of electromagnetic waves in the lower frequencies. Finally, the obtained SAR values at all the tuneable frequencies are below 1.6 W/kg for 1 g tissue. For the sake of brevity, we are only showing two lower and two higher tuneable frequencies.

6 Conclusion

In this paper, a dual-frequency reconfigurable MIMO PIFA has been presented for LTE band application in hand-held devices.

Table 2 Diversity performance of the proposed MIMO reconfigurable PIFA

Tuning band	Loading capacitor, pF	Frequency, GHz	MEG, dB			Diversity gain, dB	Channel capacity loss, bits/s/Hz	Multiplexing efficiency, dB
			MEG1	MEG2	|MEG1--MEG2|			
	4.15	0.80	−6.4523	−6.4685	0.0162	9.8	0.26	−6.9
LB	1.51	0.92	−6.1201	−6.0662	0.0539	9.85	0.23	−4.1
	0.86	0.96	−6.4045	−6.3876	0.0170	9.88	0.24	−3.2
	0.72	0.98	−6.4183	−6.4540	0.0357	9.88	0.25	−2.8
	4.15	1.65	−6.2633	−6.3134	0.0501	10	0.24	−5.2
HB	1.51	1.93	−6.2274	−6.3698	0.1424	10	0.25	−3.7
	0.86	2.10	−6.2821	−6.4622	0.1801	10	0.24	−2.4
	0.72	2.20	−6.0870	−6.0737	0.0133	10	0.25	−1.5

Table 3 Performance comparison of the proposed MIMO reconfigurable PIFA with some important references

References	MIMO environment	Tuneable bandwidth/ bandwidth	Radiating element size, mm^2	Ground size, mm^2	Antenna type	Switching element	Isolation, dB	Efficiency, %	Peak gain, dBi	SAR, W/kg	Substrate
[3]	no	880–960 MHz, 1710–1990 MHz	42×13	42×100	reconfigurable PIFA	MEMS	—	>50	>1.4	—	Rogers 4003
[4]	yes	704–787 MHz, 791–862 MHz, 2500–2690 MHz	5×125	260×200	reconfigurable PIFA	PIN diode	>20	>51	—	—	FR-4
[8]	yes	2.27–2.35 GHz	5×26	43×43	PIFA	—	>20	>50	>0.98	—	FR-4
[13]	yes	1.17 and 2.42 GHz, 0.74 and 1.03 GHz	17.7×56.6	65×120	reconfigurable PIFA	PIN diode	>12	>52	>1.37	—	Rogers 4003C
[14]	yes	755–3450 MHz	12×30	65×120	reconfigurable PIFA	PIN diode	>14	>40	>3.2	—	FR-4
[15]	yes	1.48–4.56 GHz	20×40	150×200	reconfigurable PIFA	varactor diode	>14	>79	>2.6	—	Rogers 3450
[17]	yes	0.75–0.96 GHz, 1.7–2.7 GHz	11×13	65×130	PIFA	—	—	—	—	2.7	FR-4
[19]	no	875–1013 MHz, 1700–2725 MHz	10×34	50×100	reconfigurable PIFA	PIN diode	—	>46	>−0.89	1.402	FR-4
[20]	no	880–960 MHz, 1710–1880 MHz	20×40	40×100	PIFA	—	—	>50	>2.82	1.262	FR-4
[21]	yes	0.75–0.96 GHz, 1.7–2.7 GHz	12×26	65×130	reconfigurable PIFA	MEMS switch	>10	—	—	4.2	FR-4
[26]	no	0.7–1.1 GHz, 1.7–2.3 GHz	18×36	63×100	reconfigurable PIFA	varactor diode	>20	>60	—	—	Rogers 4003C
proposed work	yes	0.8–0.98 GHz, 1.65–2.22 GHz	19×37.5	63×100	reconfigurable PIFA	varactor diode	>20	>80	>3.44	0.279	Rogers 4003C

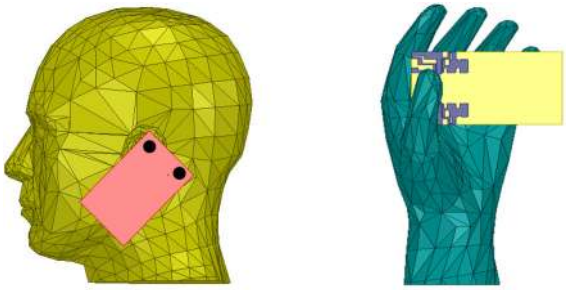

Fig. 9 *HFSS model employed to study the user proximity effect on the performance of the MIMO reconfigurable PIFA at voice position*

Using the varactor diodes, the antenna elements tune their operating frequency between 0.8–0.98 and 1.65–2.2 GHz bands. The proposed MIMO antenna consists of two symmetrical PIFAs with the centre-to-centre distance of 43 mm ($0.1906\lambda_0$) has isolation greater than 20 dB for all the tuenable frequencies. The diversity performance was evaluated by ECC, TARC, MEG, DG, CCL and multiplexing efficiency. Furthermore, the SAR distribution in a human head and hand models was investigated and found to be within acceptable SAR limit of 1.6 W/kg. Therefore, the proposed antenna is suitable to integrate multiple antennas into a limited space platform for mobile hand-held devices.

7 Acknowledgments

The authors thank Prof. Usha Kiran, for helping during the measurement of antenna in Antenna and Microwave Lab, VIT, Chennai, India. The authors thank Rogers corporation for providing the samples of the Rogers substrate. Ms Shruthi G would like to express her gratitude to the funding agency Council of Scientific and Industrial Research (CSIR) Government of India, providing financial support for research work.

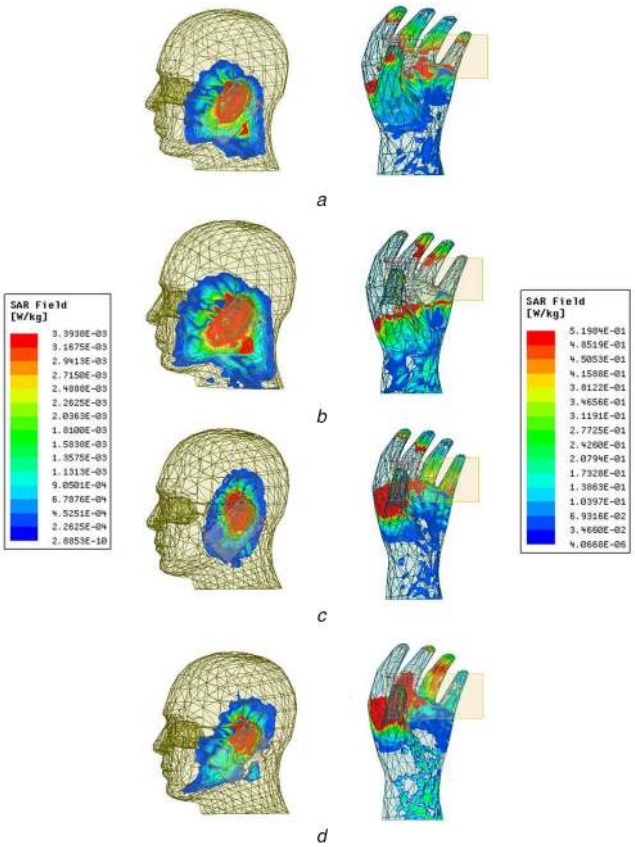

Fig. 10 *SAR performance on antenna with head model @ 15 mm and hand model*

(a) 0.86 GHz (LB tuning), ***(b)*** 0.98 GHz (LB tuning), ***(c)*** 1.72 GHz (HB tuning), ***(d)*** 2.2 GHz (HB tuning)

Table 4 Comparison of SAR and *E*-field for the proposed MIMO reconfigurable PIFA

Model	Tuning band	Tuneable frequency, GHz	Distance, mm	SAR (1 W/kg)	*E*-field, V/m
		0.86	5	0.3539	54.688
		0.98		0.3763	75.397
head	LB	0.86	10	0.2361	52.553
model		0.98		0.2983	79.187
		0.86	15	0.2217	10.119
		0.98		0.2662	87.728
		1.72	5	0.2275	23.391
		2.22		0.1403	27.040
head	HB	1.72	10	0.0704	1.8079
model		2.22		0.1167	32.682
		1.72	15	0.0508	3.1834
		2.22		0.1035	25.699
	LB	0.86	—	0.4021	8.1467
		0.98	—	0.5198	10.872
hand model					
	HB	1.72	—	0.2607	8.6443
		2.22	—	0.2794	13.984

8 References

[1] Wallace, J.W., Jensen, M.A., Swindlehurst, A.L., *et al.*: 'Experimental characterization of the MIMO wireless channel: data acquisition and analysis', *IEEE Trans. Wirel. Commun.*, 2003, **2**, (2), pp. 335–343

[2] Rowell, C., Lam, E.Y.: 'Mobile-phone antenna design', *IEEE Antennas Propag. Mag.*, 2012, **54**, (4), pp. 14–34

[3] Mak, A.C.K., Rowell, C.R., Murch, R.D., *et al.*: 'Reconfigurable multiband antenna designs for wireless communication devices', *IEEE Trans. Antennas Propag.*, 2007, **55**, (7), pp. 1919–1928

[4] Mun, B., Jung, C., Park, M., *et al.*: 'A compact frequency-reconfigurable multiband LTE MIMO antenna for laptop applications', *IEEE Antennas Wirel. Propag. Lett.*, 2014, **13**, pp. 1389–1392

[5] Jain, A., Verma, P.K., Singh, V.K.: 'Performance analysis of PIFA based 4 × 4 MIMO antenna', *Electron. Lett.*, 2012, **48**, (9), pp. 474–475

[6] Diallo, A., Luzey, C., Thuc, P.L., *et al.*: 'Study and reduction of the mutual coupling between two mobile phone PIFAs operating in the DCS1800 and UMTS bands', *IEEE Trans. Antennas Propag.*, 2006, **54**, (11), pp. 3063–3074

[7] Mohamadzade, B., Afsahi, M.: 'Mutual coupling reduction and gain enhancement in patch array antenna using a planar compact electromagnetic bandgap structure', *IET Microw. Antennas Propag.*, 2017, **11**, (12), pp. 1719–1725

[8] Chiu, C., Cheng, C., Murch, R.D., *et al.*: 'Reduction of mutual coupling between closely-packed antenna elements', *IEEE Trans. Antennas Propag.*, 2007, **55**, (6), pp. 1732–1738

[9] Chebihi, A., Luxey, C., Diallo, A., *et al.*: 'A novel isolation technique for closely spaced PIFAs for UMTS mobile phones', *IEEE Antennas Wirel. Propag. Lett.*, 2008, **7**, pp. 665–668

[10] Quevedo-Teruel, O., Inclan-Sanchez, L., Rajo-Iglesias, E.: 'Soft surfaces for reducing mutual coupling between loaded PIFA antennas', *IEEE Antennas Wirel. Propag. Lett.*, 2010, **9**, pp. 91–94

[11] Xun, J., Shi, L., Liu, W., *et al.*: 'Compact dual-band decoupling structure for improving mutual coupling of closely placed PIFAs', *IEEE Antennas Wirel. Propag. Lett.*, 2017, **16**, pp. 1985–1989

[12] Zhang, S., Lau, B.K., Tan, Y., *et al.*: 'Mutual coupling reduction of two PIFAs with a T-shape slot impedance transformer for MIMO mobile terminals', *IEEE Trans. Antennas Propag.*, 2012, **60**, (3), pp. 1521–1531

[13] Hussain, R., Sharawi, M.S.: 'Planar meandered-F-shaped 4-element reconfigurable multiple-input–multiple-output antenna system with isolation enhancement for cognitive radio platforms', *IET Microw. Antennas Propag.*, 2016, **10**, (1), pp. 45–52

[14] Hussain, R., Sharawi, M.S.: 'Integrated reconfigurable multiple-input–multiple-output antenna system with an ultra-wideband sensing antenna for cognitive radio platforms', *IET Microw. Antennas Propag.*, 2015, **9**, (9), pp. 940–947

[15] Hussain, R., Sharawi, M.S.: 'An integrated slot-based frequency-agile and UWB multifunction MIMO antenna system', *IEEE Antennas Wirel. Propag. Lett.*, 2019, **18**, pp. 2150–2154

[16] Han, K., Swaminathan, M., Pulugurtha, R., *et al.*: 'Magneto-dielectric nanocomposite for antenna miniaturization and SAR reduction', *IEEE Antennas Wirel. Propag. Lett.*, 2016, **15**, pp. 72–75

[17] Zhao, K., Zhang, S., Ying, Z., *et al.*: 'SAR study of different MIMO antenna designs for LTE application in smart mobile handsets', *IEEE Trans. Antennas Propag.*, 2013, **61**, (6), pp. 3270–3279

[18] Kwak, S.I., Sim, D., Kwon, J.H., *et al.*: 'Design of PIFA with metamaterials for body-SAR reduction in wearable applications', *IEEE Trans. Electromagn. Compat.*, 2017, **59**, (1), pp. 297–300

[19] Lee, S., Sung, Y.: 'Reconfigurable PIFA with a parasitic strip line for a hepta-band WWAN/LTE mobile handset', *IET Microw. Antennas Propag.*, 2015, **9**, (2), pp. 108–117

[20] Ikbal Hossain, M.D., Iqbal Faruque, M.R., Tariqul Islam, M.: 'Investigation of hand impact on PIFA performances and SAR in human head', *J. Appl. Res. Technol.*, 2015, **13**, (4), pp. 447–453

[21] Zhao, K., Zhang, S., Ying, Z., *et al.*: 'Adaptive quad-element multi-wideband antenna array for user-effective LTE MIMO mobile terminals', *IEEE Trans. Antennas Propag.*, 2013, **61**, (8), pp. 4275–4283

[22] Kumar, S., Kumari, R.: 'Composite right/left-handed wideband metamaterial antenna loaded with SRRs and CSRRs to improve gain and efficiency', *IET Microw. Antennas Propag.*, 2019, **13**, (9), pp. 1467–1474

[23] Zhang, S., Glazunov, A.A., Ying, Z., *et al.*: 'Reduction of the envelope correlation coefficient with improved total efficiency for mobile LTE MIMO antenna arrays: mutual scattering mode', *IEEE Trans. Antennas Propag.*, 2013, **61**, (6), pp. 3280–3291

[24] Kumar, S.M., Kumar Choukiker, Y.: 'Tunable wideband frequency and switching polarisation reconfiguration antenna for wireless applications', *IET Microw. Antennas Propag.*, 2018, **12**, (15), pp. 2364–2371

[25] 'Data sheet for varactor diode', 2018, Available at www.skyworksinc.com/Product/531/SMV1232Series

[26] Avser, B., Rebeiz, G.M.: 'Tunable dual-band antennas for 0.7–1.1-GHz and 1.7–2.3-GHz carrier aggregation systems', *IEEE Trans. Antennas Propag.*, 2015, **63**, (4), pp. 1498–1504

[27] Sharawi, M.: '*Printed MIMO antenna engineering*' (Artech House, Norwood, MA, USA, 2014)

[28] Gao, Y., Chen, X., Ying, Z., *et al.*: 'Design and performance investigation of a dual-element PIFA array at 2.5 GHz for MIMO terminal', *IEEE Trans. Antennas Propag.*, 2007, **55**, (12), pp. 3433–3441

[29] Choukiker, Y.K., Sharma, S.K., Behera, S.K.: 'Hybrid fractal shape planar monopole antenna covering multiband wireless communications with MIMO implementation for handheld mobile devices', *IEEE Trans. Antennas Propag.*, 2014, **62**, (3), pp. 1483–1488

[30] ICNIRP Guidelines: 'Guidelines on limits on exposure to radio frequency electromagnetic fields in the frequency range from 100 kHz to 300 GHz', *Health Phys.*, 1988, **54**, pp. 115–123